ACS APPLIED MATERIALS & INTERFACES

Research Article

www.acsami.org

Noncovalent Ruthenium(II) Complexes–Single-Walled Carbon Nanotube Composites for Bimodal Photothermal and Photodynamic Therapy with Near-Infrared Irradiation

Pingyu Zhang, Huaiyi Huang, Juanjuan Huang, Hongmin Chen, Jinquan Wang, Kangqiang Qiu, Donglei Zhao, Liangnian Ji, and Hui Chao*

MOE Key Laboratory of Bioinorganic and Synthetic Chemistry, School of Chemistry and Chemical Engineering, Sun Yat-Sen University, Guangzhou 510275, People's Republic of China

Supporting Information

ABSTRACT: To enhance the efficacy and optimize the treatment of cancers, the integration of multimodal treatment strategies leading to synergistic effects is a promising approach. The coassembly of multifunctional agents for systematic therapies has received considerable interest in cancer treatment. Herein, Ru(II) complex-functionalized single-walled carbon nanotubes (Ru@SWCNTs) are developed as nanotemplates for bimodal photothermal and two-photon photodynamic therapy (PTT-TPPDT). SWCNTs have the ability to load a great amount of Ru(II) complexes (**Ru1** or **Ru2**) via noncovalent $\pi-\pi$ interactions. The loaded Ru(II) complexes are efficiently released by the photothermal effect of irradiation from an 808 nm diode laser (0.25 W/cm^2). The released Ru(II) complexes produce singlet oxygen species ($^1O_2$) upon two-photon laser irradiation (808 nm, 0.25 W/cm^2) and can be used as a two-photon photodynamic therapy (TPPDT) agent. Based on the combination of photothermal therapy and two-photon photodynamic therapy, Ru@SWCNTs have greater anticancer efficacies than either PDT using Ru(II) complexes or PTT using SWCNTs in two-dimensional (2D) cancer cell and three-dimensional (3D) multicellular tumor spheroid (MCTS) models. Furthermore, *in vivo* tumor ablation is achieved with excellent treatment efficacy under a diode laser (808 nm) irradiation at the power density of 0.25 W/cm^2 for 5 min. This study examines an efficacious bimodal PTT and TPPDT nanoplat form for the development of cancer therapeutics.

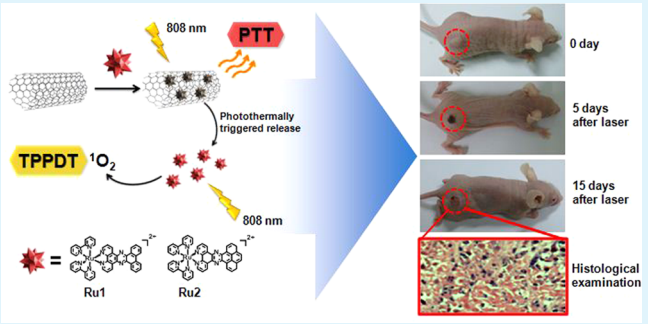

KEYWORDS: *photothermal therapy, photodynamic therapy, two-photon, Ru(II) complex, single-walled carbon nanotubes*

INTRODUCTION

Among all anticancer treatments, photodynamic therapy (PDT) and photothermal therapy (PTT), involving the use of visible or near-infrared (NIR) light, have unique advantages, including remote controllability, low systemic toxicity, and few side effects.[1−6] The ideal clinical phototherapeutic window for tumors is between 700 nm and 1100 nm,[7] where the attenuation of light by blood and soft tissues is low, allowing for the treatment of deep-seated tumors. For PDT, light-activated photosensitizers (PSs) can generate reactive oxygen species, such as singlet oxygen ($^1O_2$), free radicals, and peroxides, which can irreversibly damage tumor tissues.[8] Unfortunately, most available PSs, such as hemoporphyrin and phthalocyanine, absorb light energy only over wavelengths shorter than 600 nm, which is a serious drawback for efficacious PDT. Thus, many studies have focused on the design of new PSs or the chemical modification of existing PSs with large absorption cross sections in the NIR region.[9] The implementation of PTT relies on the development of photothermal coupling agents. Carbon nanomaterials, such as graphene, single-walled carbon nanotubes (SWCNTs), and single-wall carbon nanohorns (SWCNHs), have become increasingly popular for photothermal therapy.[10,11] Pioneering studies have shown that SWCNTs can be used to deliver therapeutic drugs and diagnostic molecules into cells.[12−20] SWCNTs can also absorb light in the near-infrared region and can cause cell death by localized photothermal effects.[21] The use of SWCNTs would help develop innovative multimodal therapies that combine PTT and photodynamic therapy (PDT). Because PDT is a noninvasive phototherapy currently used in clinical practice,[22−24] the combination of PTT with PDT is feasible and has clinical value.

Many metal complexes (e.g., Ru(II) complexes, Ir(III) complexes) are thought as wonderful therapeutic agents.[25−27] The use of Ru(II) complexes for PDT therapy has gained great interest in recent years. Most studies have reported that Ru(II) polypyridyl complexes efficiently produce $^1O_2$ upon irradiation with UV or visible light[28−30] and exhibit high phototoxic

Received: August 13, 2015
Accepted: October 2, 2015
Published: October 2, 2015

DOI: 10.1021/acsami.5b07510
ACS Appl. Mater. Interfaces 2015, 7, 23278−23290

Scheme 1. Schematic Design of Ru@SWCNTs for Bimodal Photothermal Therapy (PTT) and Two-Photon Photodynamic Therapy (TPPDT) with 808 nm Irradiation

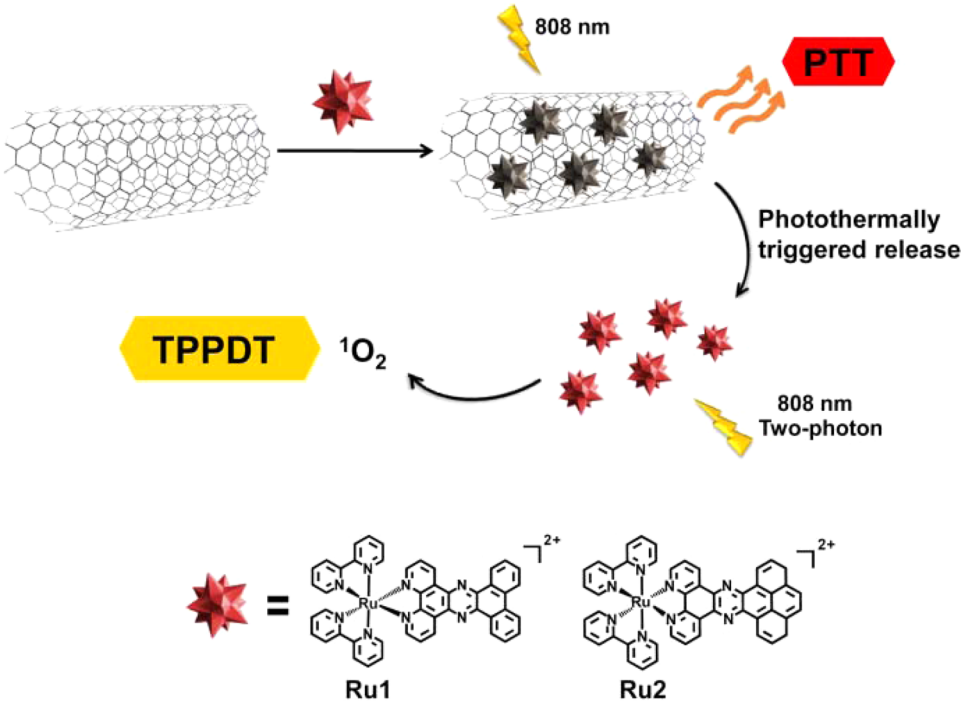

indices in metastatic melanoma models.[31] In our previous work, we found Ru(II) polypyridyl complexes had strong two-photon absorbing and luminescence properties, deep tissue penetration and unique spatial resolution.[32−34] These promising results have led us to further develop Ru(II) polypyridyl complexes as two-photon photodynamic anticancer agents. The combination of PDT with two-photon absorbing photosensitizers in the NIR therapeutic window can offer new prospects for cancer treatment.

To determine if bimodal PDT and TPPTT can be used as a more effective cancer therapy, we load two-photon luminescent Ru(II) complexes as TPPDT agents onto SWCNTs. We find that the temperature of Ru@SWCNTs significantly increases to ∼58 °C under 808 nm laser irradiation at 0.25 W/cm^2. Furthermore, the photothermal effect triggers the release of Ru(II) complexes, and the released Ru(II) complexes produce $^1O_2$ upon the two-photon laser irradiation (808 nm). Bimodal TPPDT and PTT therapy using Ru@SWCNTs has greater anticancer effects than either PDT using Ru(II) complex or PTT using SWCNTs. Ru@SWCNTs can be used as a bimodal PTT/TPPDT therapy system (Scheme 1).

RESULTS AND DISCUSSION

Synthesis and Characterization. The Ru@SWCNTs were readily formed by sonicating Ru(II) complexes with SWCNTs solutions for 4 h at room temperature, followed by repeated washes to remove free Ru(II) complexes. The characteristics of Ru@SWCNTs were compared with those of SWCNTs dispersed in an aqueous solution of SDS ionic surfactants (because SWCNTs were not water-soluble).[35] The morphology of the Ru@SWCNTs hybrid system was characterized by transmission electron microscopy (TEM). Initial insights into the formation of Ru@SWCNTs adducts were obtained by comparing the pristine and Ru(II) complex-modified SWCNTs (Figure 1 and Figure S1 in the Supporting Information). As shown in Figure 1a and Figure S1a, the pristine SWCNTs had very smooth surfaces, with diameters of ∼0.7−1.3 nm. The lengths of the Ru@SWCNTs ranged from 20 nm to several micrometers. After the Ru(II) complex modification, surface roughness was clearly observed on the sidewalls of the SWCNTs corresponding with the adsorption of Ru(II) complexes loading onto the SWCNTs by $\pi-\pi$ interaction (see Scheme S1 in the Supporting Information). It was feasible for carbon nanoparticles to noncovalently $\pi-\pi$ stack with water-soluble planar aromatic molecules to implement multifunctions.[35,36]

The absorption spectra of SWCNT showed a strong broad NIR absorption (Figure 1b and Figure S1b). After the Ru(II) complex modification, the MLCT absorbance band appeared at ∼450 nm, and the NIR absorption band was also present. Figure 1c and Figure S1c gave the Raman spectra of pristine SWCNTs, Ru(II) complexes, and Ru@SWCNTs. The Raman spectra of both pristine SWCNTs and Ru@SWCNTs showed two bands at 1340 cm^{-1} (D-band) and 1584 cm^{-1} (G-band), which were indicative of surface defects and the sp^2 hybridized carbon stretching vibrations of SWCNTs, respectively. Moreover, a weak peak, assigned to the C═C stretching mode of Ru(II) complexes at ∼1444 cm^{-1}, appeared in the Raman spectra of Ru@SWCNTs. Compared with SWCNTs, Ru@SWCNTs had asignificantly higher water solubility. The Ru@SWCNTs had great stability when they were stored in H_2O, PBS or DMEM with 10% FBS at room temperature over a period of 3 months (see Figures S2 and S3 in the Supporting Information). Thus, the Ru(II) complex modification did not affect the spectral characteristics of SWCNTs, but did increase their physical stability.

The elemental composition of Ru@SWCNTs was determined via X-ray photoelectron spectroscopy (XPS) measurements (see Figures S4 and S5 in the Supporting Information). The results provided the chemical composition and the energy

DOI: 10.1021/acsami.5b07510
ACS Appl. Mater. Interfaces 2015, 7, 23278−23290

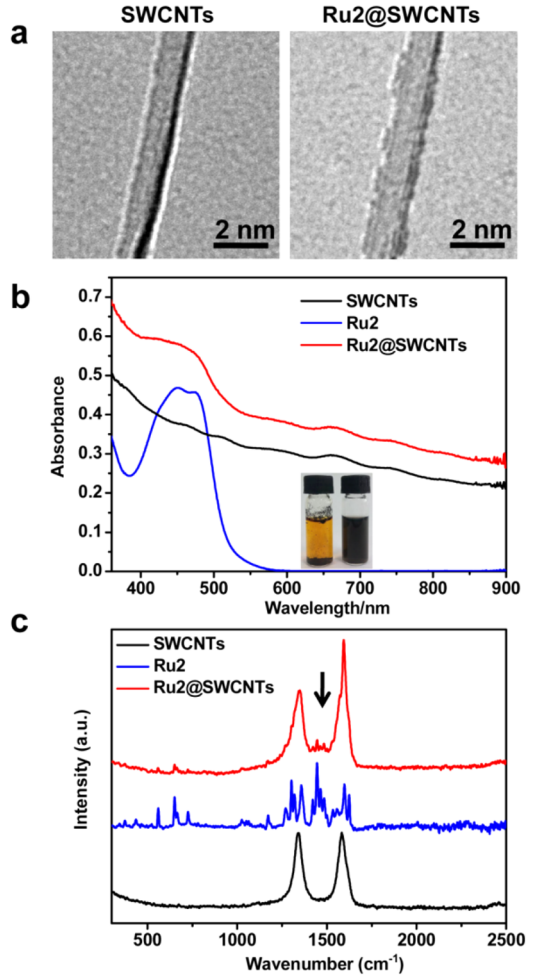

Figure 1. (a) Transmission electron microscopy (TEM) images of the synthesized Ru2@SWCNTs. (b) UV-vis spectra of Ru@SWCNTs, **Ru2** and SWCNTs in aqueous solution, SWCNTs were dispersed in an aqueous solution of the SDS ionic surfactants, because of the insolubility of SWCNTs. (c) Raman spectra of Ru2@SWCNTs, **Ru2** and SWCNTs. Inset: photographs showed the SWCNTs and **Ru2** dispersed in aqueous solution before and after sonication.

distribution of C_{1s}, Ru_{3d}, N_{1s} and Cl_{2p}, which indicated that the Ru(II) complex was successfully modified onto the SWCNTs. We also used inductively coupled plasma mass spectrometry (ICP-MS) analysis to quantitatively determine the concentration of the Ru(II) complex in a 50 μg/mL Ru@SWCNTs aqueous suspension (see Table S1 in the Supporting Information). The concentration of the **Ru1** complex for the Ru1@SWCNT composites was 13.5 μg/mL, and the concentration of SWCNT was 36.5 μg/mL. The concentration of the **Ru2** complex for the Ru2@SWCNT composites was 15.4 μg/mL, and the concentration of SWCNT was 34.6 μg/mL. The results showed that, for larger π conjugates of the Ru(II) complex, more Ru(II) complexes were modified onto the SWCNTs.

Photothermal Properties of the Ru@SWCNT. We investigated the photothermal therapy potential of the nanocomposites. A diode laser (808 nm) was used at a power density of 0.25 W/cm^2 to irradiate water, pure SWCNTs, and the Ru@SWCNTs (100 μL, 50 μg/mL) for different durations (0−5 min). We then used a thermal imaging camera to record the temperature variation every 30 s (Figure 2). The thermal signals of pure water showed no obvious change (ΔT < 2 °C). The SWCNTs were shown to convert

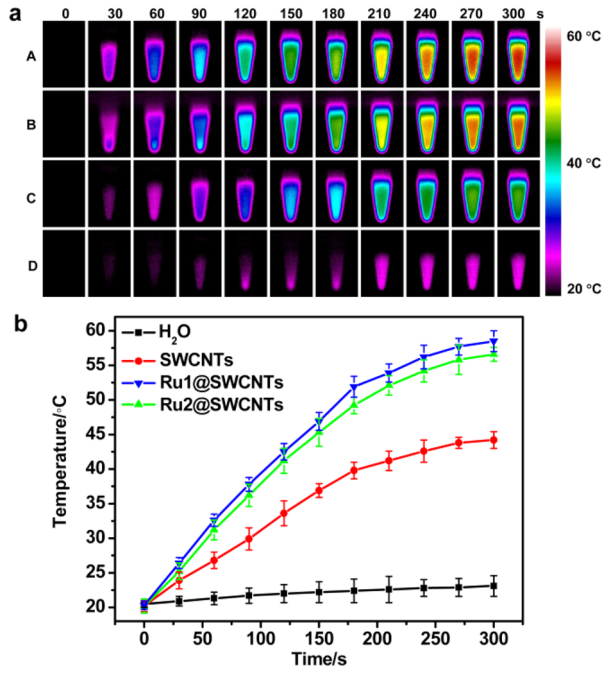

Figure 2. (a) Photothermal images of the nanoparticle solutions at the same concentration (100 μL, 50 μg/mL) and irradiation time (0−5 min): (A) Ru1@SWCNTs, (B) Ru2@SWCNTs, (C) SWCNTs, and (D) H_2O (the power of the 808 nm laser was 0.25 W/cm^2). (b) The temperature change of the Ru@ SWCNTs as a function of irradiation time; H_2O and pure SWCNTs are used as controls.

NIR light to heat (from 20.2 °C to 44.2 °C). However, these temperature increases (ΔT) of the Ru@SWCNTs were much higher (from 20.3 to 58.5 °C for Ru1@SWCNTs and from 20.2 to 56.6 °C for Ru2@SWCNTs) under the same experimental conditions. The phothotherml conversion efficiency of Ru@SWCNTs is ∼39.4% (for Ru1@SWCNTs) and 38.3% (for Ru1@SWCNTs), which is higher than gold nanoparticles (gold nanorods, η = 22.0%; gold nanostars, η = 18.9%[37,38]) and Cu_9S_5 nanocrystals (η = 25.7%[39]). When the Ru1@SWCNTs concentration was fixed at 50 μg/mL, an obvious power-density-dependent temperature rise was observed (see Figure S6 in the Supporting Information). A temperature increase to >50 °C could be obtained with an incident laser power as low as 0.25 W/cm^2. The laser power used in the present study was lower than 0.33 W/cm^2 at 808 nm (ANSI Z136.1; 2007, American National Standard for Safe Use of Lasers) and even lower than those of a few recent reports.[40−45] The temperature increase was well above the required temperature rise for efficient cancer photothermal therapy.[46] These results clearly suggested that Ru@SWCNTs can act as an efficient photothermal therapy agent.

Photothermal-Triggered Release of Ru(II) Complexes. After irradiation, we found that Ru(II) complexes could be released from Ru@SWCNTs via photothermal triggers. After an initial dose of irradiation from an 808 nm diode laser (First) at 0.25 W/cm^2 output power for 5 min, the cumulative release, defined as the ratio of released Ru(II) complex to total loaded Ru(II) complex, increased from 2.1% to 52.5% for Ru1@SWCNTs and from 1.0% to 55.4% for Ru2@SWCNTs (Figure 3). The release of Ru(II) complexes completely stopped when

DOI: 10.1021/acsami.5b07510
ACS Appl. Mater. Interfaces 2015, 7, 23278−23290

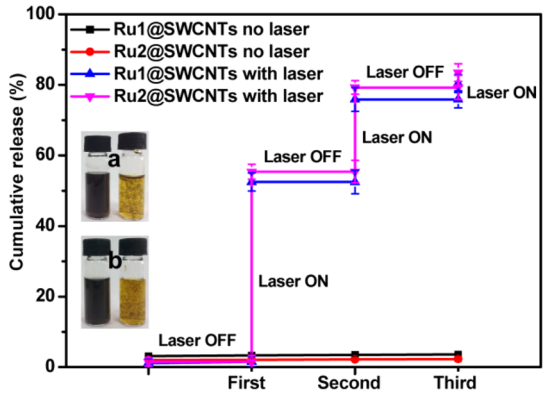

Figure 3. Photothermal-triggered release of Ru(II) complexes from Ru@SWCNTs. Ru(II) complex release profiles in the presence and absence of laser irradiation. Irradiation with 808 nm laser caused rapid Ru(II) complex release during laser exposure (5 min), and the release was turned off when laser was switched off (20 min). The process was repeated three times. The cumulative released Ru(II) complex was measured. Inset: photographs showing (a) the Ru1@SWCNTs and (b) the Ru2@SWCNTs before and after irradiation in aqueous solution.

the 808 nm laser was switched off. Similar results were observed when the laser treatment protocol was repeated (Second). However, there were fewer Ru(II) complexes released during the second treatment cycle. By the third cycle (Third), almost no Ru(II) complexes were released.

The UV-vis absorption qualitatively also proved that the Ru(II)complex was almost completely released from Ru2@SWCNTs after irradiation (see Figure S7 in the Supporting Information). The UV-vis absorption of the centrifugal liquid corresponded to the spectrum of Ru(II) complex itself, and the centrifugal solid comprised SWCNTs. We further examined the centrifugal liquid and centrifugal solid by quantitative tests. The centrifugal liquid and centrifugal solid was isolated and characterized by ICP-MS measurements (Table S1 in the Supporting Information). Ru (from the Ru(II) complex) were abundant in the centrifugal liquid. However, in the centrifugal solid, the amounts of Ru dramatically decreased, and almost no residues remained on the SWCNTs surfaces. These data suggested that the Ru(II) complexes released from the Ru@SWCNTs could be triggered by the photothermal effect due to 808 nm laser irradiation.

Photophysical Properties. We monitored the emission behavior of Ru@SWCNTs. The strong emissions of the Ru(II) complexes were almost completely quenched (95.8%−99.5%) after interacting with the SWCNTs (Figure S8 in the Supporting Information). The free Ru1 or Ru2 complexes exhibited strong luminescence at ∼610 nm, with luminescence quantum yields (Φ_{em}) of 0.014−0.016 (see Table 1) using $[Ru(bpy)_3]^{2+}$ (Φ_{em} = 0.028 in water[47]) as a reference. To determine their lifetimes, a luminescent decay experiment was performed at 298 K, which showed that the lifetimes of the Ru1 and Ru2 complexes were 356−405 ns (see Table 1). These lifetimes were obtained by fitting the data to single exponential decay functions. Next, the two-photon luminescence (TPL) properties of the Ru(II) complexes were investigated by determining the two-photon absorption cross-section δ (TPA) of Ru1 and Ru2 using Rhodamine B as a reference (see Table 1 and Figure S9a in the Supporting Information). Ru1 and Ru2 exhibited strong two-photon emissions upon 808 nm excitation (Ru1: $\delta_{808\ nm}$ = 494; Ru2: $\delta_{808\ nm}$ = 428 Göppert−Mayer (GM); 1 GM = 1×10^{-50} $cm^4\ s^{-1}$ $photon^{-1}$). The two-photon excitation active process was confirmed via a power-dependence experiment. A log−log linear relationship between the emission intensity and incident power with a gradient showed the best fit ($n \approx 2$) (Figure S9b).

Singlet Oxygen Sensitization. We further employed electron paramagnetic resonance (EPR) spectroscopy and spin trapping to detect ROS generation by the Ru(II) complexes under 808 nm laser irradiation (0.25 W/cm^2, 80 MHz, 100 fs). 2,2,6,6-Tetramethylpiperidine (TEMP) and 5,5-dimethyl-1-pyrroline-*N*-oxide (DMPO) were used as $^1O_2$ and $O_2\cdot$ (or OH·) trappers, respectively. As illustrated in Figure 4

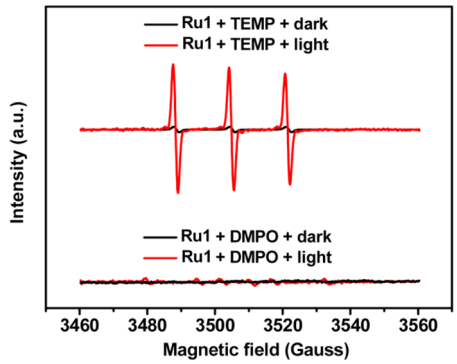

Figure 4. EPR signals of $^1O_2$ (top) and other ROS (bottom) obtained with or without 808 nm laser irradiation (0.25 W/cm^2) of Ru(II) complex (**Ru1**) for 5 min in the presence of 2,2,6,6-tetramethylpiperidine (TEMP) and 5,5-dimethyl-1-pyrroline-*N*-oxide (DMPO), respectively.

and Figure S10 in the Supporting Information (top, red line), a characteristic $^1O_2$-induced signal, 2,2,6,6-tetramethylpiperidine-1-oxyl, was observed in the EPR spectra only under irradiation. However, no other ROS signals were observed (Figure 4, bottom). These results verified that it was the energy transfer (ET), not the electron transfer, from the Ru(II) complex to oxygen that was responsible for the sensitization of ground-state oxygen. To assess the ability of the Ru(II) complex to

Table 1. Photophysical Data and Singlet Oxygen Quantum Yields of Ru1 and Ru2

					Φ ($^1O_2$)[d]		$\delta \times \Phi$ ($^1O_2$) [GM][e]	
complex	λ_{abs} [nm] (ε [$\times 10^{-3}$ M^{-1} cm^{-1}])[a]	λ_{em} [nm] (Φ_{em} [%])[a]	τ [ns][b]	δ [GM][c]	indirect	direct	indirect	direct
Ru1	448 (23.5)	614 (1.6)	356	494	0.33	0.35	163.0	172.9
Ru2	445 (25.4)	611 (1.4)	405	428	0.30	0.31	128.4	132.7

[a]Absorbance and emission spectra recorded in water at room temperature; Φ_{em} refer the fluorescence quantum yield, the standard was $[Ru(bpy)_3]^{2+}$ (Φ_{em} = 0.028 in water).[47] [b]τ refer to the lifetime and evaluated in water. [c]δ refer to the two-photon absorption cross-section and evaluated in water. [d]Φ ($^1O_2$) was detect in D_2O by indirect and direct methods, the standard was $[Ru(bpy)_3]^{2+}$ (Φ^s_Δ = 0.22 in D_2O).[48] [e]Figure of merit for two-photon singlet oxygen sensitization.[50,51]

DOI: 10.1021/acsami.5b07510
ACS Appl. Mater. Interfaces 2015, 7, 23278−23290

generate $^1O_2$, the $^1O_2$ quantum yield was measured using two different methods with $[Ru(bpy)_3]^{2+}$ as the standard photosensitizer ($^1O_2$ quantum yield Φ_Δ = 0.22 in D_2O[48]): (1) by monitoring the absorbance variations of a probe molecule caused by a trapped $^1O_2$ adduct (i.e., an indirect evaluation), and (2) by direct measurement of the infrared phosphorescence of $^1O_2$.[28−30] The first method was based on the reaction of $^1O_2$ with a singlet oxygen sensor (DPBF, 1,3-diphenyliso-benzofuran)[49] (Figure S11 in the Supporting Information).

The second method was applied in the presence of $^1O_2$ and assessed directly by the detection of its phosphorescence at 1270 nm (Figure S12 in the Supporting Information). In our case, the $^1O_2$ production quantum yields were determined to be 0.30−0.35 upon one-photon 450 nm excitation for these two methods (Table 1). The two-photon singlet oxygen sensitization was based on the quantum yield of a one-photon excited singlet oxygen generation and the two-photon absorption cross-section. Thus, $\delta \times \Phi_\Delta(^1O_2)$ showed singlet oxygen generation by two-photon excitation.[50,51] The $\delta \times \Phi_\Delta$ ($^1O_2$) values of **Ru1** and **Ru2** (128.4−172.9 GM, Table 1) were much larger than that of H_2TPP (1.5 GM),[51] indicating the excellent performance of **Ru1** and **Ru2** as two-photon singlet oxygen sensitizers.

Two-Photon-Induced $^1O_2$ Generation in Cancer Cells. To demonstrate that the released Ru(II) complex could produce singlet oxygen *in vitro* after 808 nm laser irradiation, we incubated HeLa cells with the Ru(II) complex (50 μg/mL) and the 2,7-dichlorodihydrofluorescein diacetate (DCFH-DA). Once in the cells, DCFH-DA is hydrolyzed by esterase enzymes to DCF, which is vulnerable to singlet oxygen and can be oxidized to the fluorescent compound 2,7-dichlorofluorescein (DCF). DCFH-DA has been widely used to assess the production of $^1O_2$ in living cells.[30] We recorded the confocal fluorescence images of the cells before and after the 2 min 808 nm two-photon laser irradiation via a confocal microscope equipped with a mode-locked Ti:sapphire laser source (0.25 W/cm^2, 80 MHz, 100 fs). Cells treated with only the DCFH-DA control showed no obvious fluorescence enhancement following irradiation. In contrast, a significant fluorescence increase was observed following irradiation in the cells treated with both the Ru(II) complex/Ru@SWCNTs and DCFH-DA (see Figure 5 and Figure S13 in the Supporting Information). The fluorescence was very weak in the presence of 10 mM *N*-acetylcysteine (NAC, an antioxidant, does not react with Ru(II) complex/Ru@SWCNTs) before the cells were treated. This finding suggested that Ru(II) complexes/Ru@SWCNTs were efficient two-photon absorbing photosensitizers in the cells.

Cellular Uptake Analysis. As described above, the photothermal effect on Ru@SWCNTs could trigger Ru(II) complex release. To explore the action of Ru@SWCNTs in HeLa cells, we traced the cellular two-photon luminescence of the Ru@SWCNTs in dark conditions and under an 808 nm laser irradiation (0.25 W/cm^2, 80 MHz, 100 fs) by two-photon confocal laser microscopy (Figure S14a in the Supporting Information). Without 808 nm irradiation, only weak red fluorescent spots were found in the HeLa cells. However, after the laser irradiation for 2 min (the time was decreased because cell death occurs with excessive irradiation exposure, i.e., 5 min) in the Ru@SWCNTs treated cells, the strong red two-photon luminescence (λ_{ex} = 808 nm, two-photon laser) was observed as more diffused spots in the lysosomes, which co-localized well with the green fluorescence emanating from Lyso-Tracker (the overlap coefficient was 82.5%). This result implied that

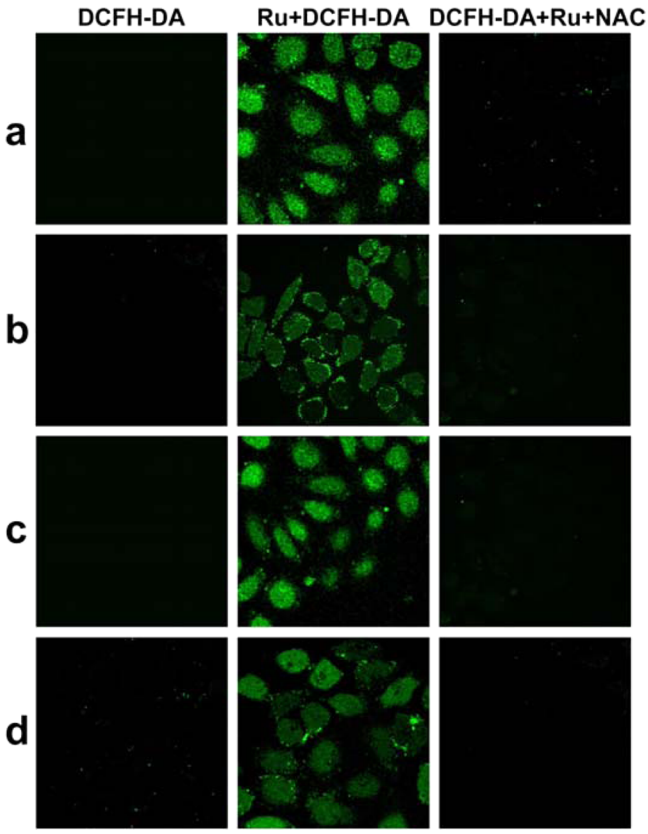

Figure 5. Intracellular $^1O_2$ measurements. HeLa cells were incubated with the DCFH-DA (10 μM) in the absence or in the presence of (a) **Ru1**, (b) **Ru2**, (c) Ru1@SWCNTs, and (d) Ru2@SWCNTs. The concentration of NAC was 10 mM. The samples were irradiated for 2 min with two-photon laser irradiation (0.25 W/cm^2).

endocytosis was responsible for the uptake of the Ru@SWCNTs. The TEM images also supported an endocytosis mechanism for the uptake of the Ru@SWCNTs and showed that the Ru@SWCNTs formed endosomes in the cells (Figure S14b). These observations indicated that Ru@SWCNTs were successfully engulfed by lysosomes. After 808 nm irradiation, the photothermal effect triggered the release of Ru(II) complexes and strong two-photon luminescence was observed in the cancer cells.

PTT−TPPDT Combined Therapy in Two-Dimensional (2D) Cancer Cells. We next tested PTT−TPPDT combined therapy in cellular experiments using HeLa cancer cells. Cells were incubated with Ru(II) complexes, SWCNTs, and Ru@SWCNTs at a series of concentrations for 24 h and then irradiated with an 808 nm laser at a power density of 0.25 W/cm^2 for 5 min. A standard methyl thiazolyltetrazolium (MTT) assay was carried out to determine the relative viabilities of the cells 24 h after various treatments be been performed. Without laser exposure, Ru@SWCNTs, SWNTs, and the free Ru(II) complex all exhibited negligible dark toxicity to HeLa cancer cells and LO2 normal cells (see Figure 6a and Figure S15 in the Supporting Information). HeLa cells also exhibited no loss of viability after being irradiated in the absence of the Ru@SWCNTs (control + laser, Figure 6b). This finding indicated that the untreated cells remained safe under irradiation of 0.25 W/cm^2 laser power. Surprisingly, the cancer cell killing effect of Ru@SWCNTs when irradiated by the 808 nm laser was remarkably higher than that of free Ru(II) complex and

DOI: 10.1021/acsami.5b07510
ACS Appl. Mater. Interfaces 2015, 7, 23278−23290

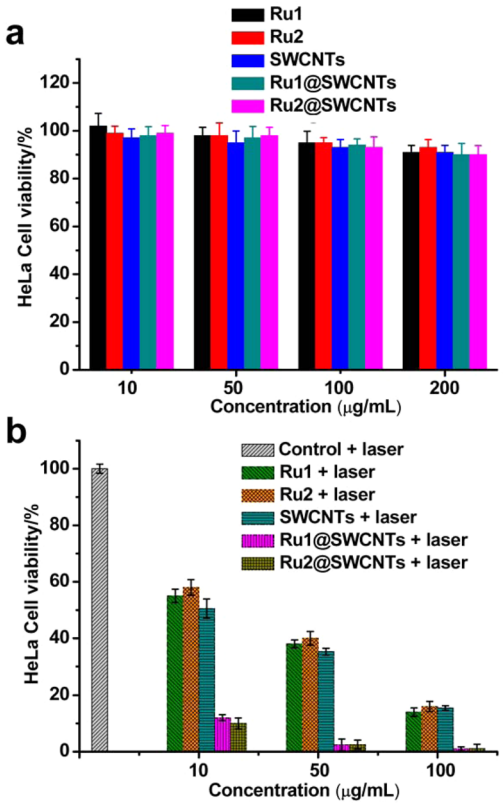

Figure 6. (a) Percentage of HeLa cell viability after the treatment with Ru complexes, SWCNTs and Ru@SWCNTs in different concentration (10, 50, 100, 200 μg/mL) for 24 h without laser irradiation. The untreated cells were considered to have 100% survival. (b) Viability of HeLa cells after the treatment with Ru complexes, pure SWCNTs and Ru@SWCNTs induced photothermal therapy and two-photon photodynamic therapy upon 808 nm laser irradiation (0.25 W/cm^2, 5 min).

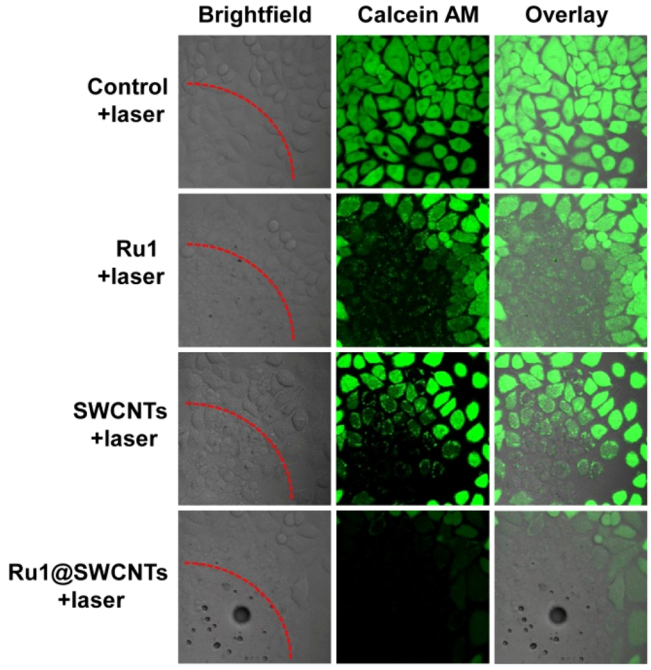

Figure 7. Images of the HeLa cells observed by fluorescence microscopy after incubating with the dye Calcein AM (green, λ_{ex} = 488 nm, λ_{em} = 520 ± 20 nm). Four groups: Control + laser; **Ru1** (13.5 μg/mL) + laser; SWCNTs (36.5 μg/mL) + laser; Ru1@SWCNTs (50 μg/mL) + laser. The laser wavelength was 808 nm (0.25 W/cm^2).

SWCNTs (Figure 6b). The Ru(II) complex and SWCNTs mixture as a control also showed lower photothermal effect than Ru@SWCNTs (Figure S16 in the Supporting Information). The PTT−TPPDT effect of the Ru@SWCNTs was then monitored via calcein AM staining assay (Figure 7 and Figure S17 in the Supporting Information). Viable cells were stained green with calcein AM. HeLa cells treated with the Ru@SWCNTs (50 μg/mL) followed by 808 nm laser irradiation (0.25 W/cm^2 for 5 min) died (as represented by the significant reduction of green fluorescence). All other groups and control cells showed no observable damage to the cancer cells. Cells treated with al aser and Ru(II) complex/SWCNTs showed stronger green fluorescence than Ru@SWCNTs. The results indicated that Ru@SWCNTs destroyed cancer cells more efficiently, compared with free SWCNTs and Ru(II) complexes, which can be attributed to bimodal PTT and TPPDT from the Ru@SWCNTs composites.

PTT−TPPDT Combined Therapy in Three-Dimensional (3D) Multicellular Tumor Spheroids (MCTSs). Two-dimensional (2D) cultures of adherent cells are routinely used in numerous areas of the biomedical and life sciences. However, this model presents significant limitations in reproducing the complexity and pathophysiology of *in vivo* solid tumors.[52] Multicellular tumor spheroids (MCTSs) are heterogeneous cellular aggregates and have been gradually accepted as valid 3D cancer models that connects cell monolayers and solid tumors.[53−57] Because of this, we decided to test the photothermal therapy of the Ru@SWCNTs against MCTSs with diameters of ~400 μm. We observed the effects of Ru@SWCNTs-based PTT−TPPDT on the kinetics of 3D tumor regrowth (Figure 8). After treatment with Ru@SWCNTs (50 μg/mL) alone, there were no observed differences in MCTSs over a period of 1 day. The untreated MCTSs showed no difference after 808 nm laser (0.25 W/cm^2) irradiation. However, the MCTSs treated with Ru@SWCNTs and 5 min laser irradiation indicated that the diameter of MCTSs became smaller over time.

To verify if the MCTSs were living or dead, a calcein AM staining assay was performed to further determine the viability (Figure 8c). As expected, Ru@SWCNTs with an 808 nm laser-induced cell death in the MCTSs, as indicated by the weak green fluorescence. However, the cells in the MCTS control were alive, as indicated by the strong green fluorescence of calcein in the entire MCTS. The cytotoxicity test also indicated that the cell viabilities of the Ru@SWCNTs without irradiation were >96%. After 5 min of laser irradiation, the cell viabilities of the MCTSs were only 5% (Figure 8d). All data indicated that Ru@SWCNTs exhibited excellent bimodal photothermal and photodynamic therapy effect in 3D MCTS cancer models.

Photothermal Therapy *In Vivo*. We further attempted to study the *in vivo* photothermal therapy efficacy of our Ru@SWCNTs. At this stage, note that the preferred route of photothermal conversion agents (PTCAs) administration in photothermal cancer therapy is intratumoral injection, instead of intravenous injection.[58−61] Nie et al. recently reported that active molecular targeting of the tumor microenvironments (e.g., fibroblasts, macrophages, and vasculatures) did not significantly influence the tumor nanoparticle uptake when the nanoparticles were administered via intravenous injection.[62] Therefore, we opted in the present study for intratumoral

DOI: 10.1021/acsami.5b07510
ACS Appl. Mater. Interfaces 2015, 7, 23278−23290

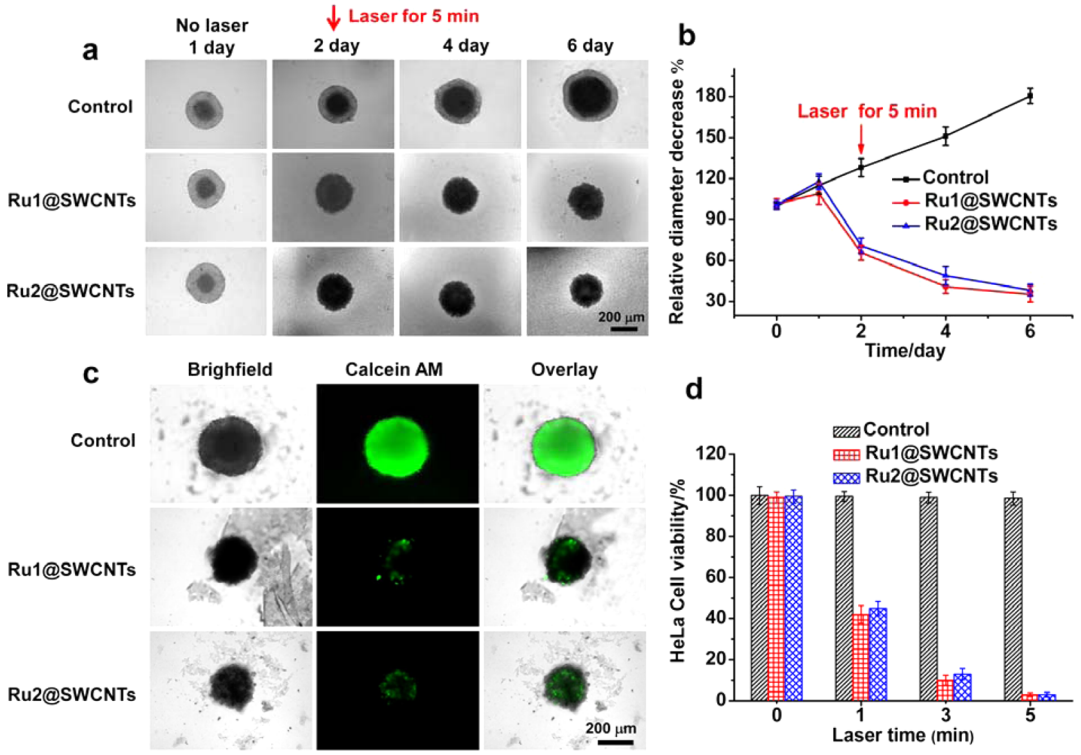

Figure 8. (a, b) Diameter change of Ru@SWCNTs (50 μg/mL) and irradiation incubated with tumor spheroids by increasing days. (c, d) Percentage of 3D HeLa cells viability and live/dead assay after the cells treatment with Ru@SWCNTs and 808 nm laser irradiation (0.25W/cm^2) for 72 h, untreated cells were considered to have 100% survival.

injection to assess the *in vivo* PPT potential of our Ru@SWCNTs.

To assess their *in vivo* therapeutic potential, nude mice bearing the HeLa tumor model were injected intratumorally with 100 μL of aqueous dispersion of 1 mg/mL of Ru@SWCNTs or blank physiological saline, and the tumors were then exposed to 808 nm laser at a power density of 0.25 W/cm^2 for 5 min. As shown in Figure 9, the temperature of the tumor regions with Ru@SWCNTs increased rapidly from 36.5 °C to 62.8 °C (Ru1@SWCNTs) or 59.5 °C (for Ru2@SWCNTs) in 5 min. In contrast, tumors injected with blank and laser only showed a temperature change of ~5 °C after the same laser irradiation treatment. During 15 days of observation, the tumors on injected mice were ablated after photothermal treatment without regrowth or with rather slow growth. The tumors were shrinking gradually or even disappeared individually after 15 days of treatment (see Figures 10a and 11). In contrast, tumors in the control mice that received laser alone/Ru@SWCNTs alone treatment continued to grow rapidly, and all of these mice had to be euthanized after 15 days. Histological examination of tumor was performed after the photothermal therapy treatment (Figure 10b). As expected, in the mice treated with the Ru@SWCNTs followed by laser irradiation, the tumor tissues were necrotic, exhibiting pyknosis, karyolysis, and degradation. In contrast, the tumor tissues of the control group exhibited a normal organized cellular structure.

To determine whether the treatments induced toxicity, we monitored the body weight of the mice (Figure S18 in the Supporting Information) and the histology of organs including the intestine, lung, liver, ovary, brain, spleen, kidney, and heart (Figure S19 in the Supporting Information). The body weight of the mice treated with the Ru@SWCNTs under a diode laser (808 nm) irradiation at the power density of 0.25 W/cm^2 was

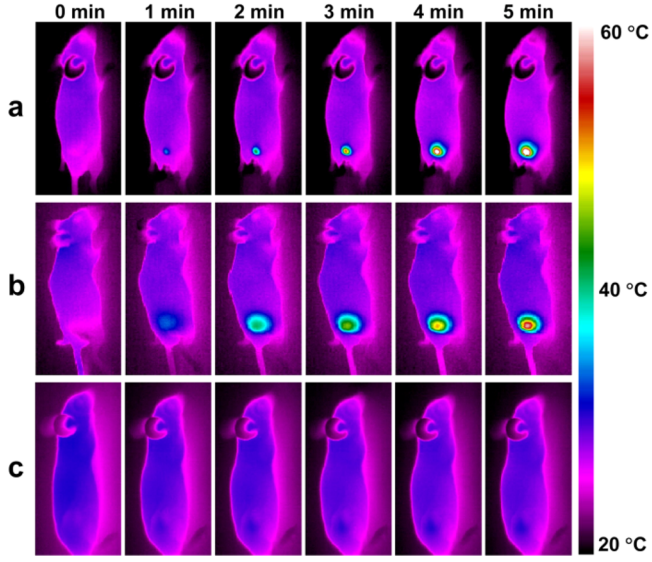

Figure 9. Thermographs of tumor-bearing mice receiving photothermal treatment for different periods of time (0−5 min). The mice were injected intratumorally with (a) Ru1@SWCNTs, (b) Ru2@SWCNT, and (c) control.The laser power density was 0.25 W/cm^2.

no different than that of the control. No body weight loss and other serious toxic effects were observed. In addition, histological analysis did not reveal any serious irreversible pathological alterations or injuries in the organs of mice of all groups. This strongly suggested that the Ru@SWCNTs medicated photothermal ablation was not inducing any toxicity. All results clearly indicated that the Ru@SWCNTs acted as powerful photothermal agents *in vivo*.

DOI: 10.1021/acsami.5b07510
ACS Appl. Mater. Interfaces 2015, 7, 23278−23290

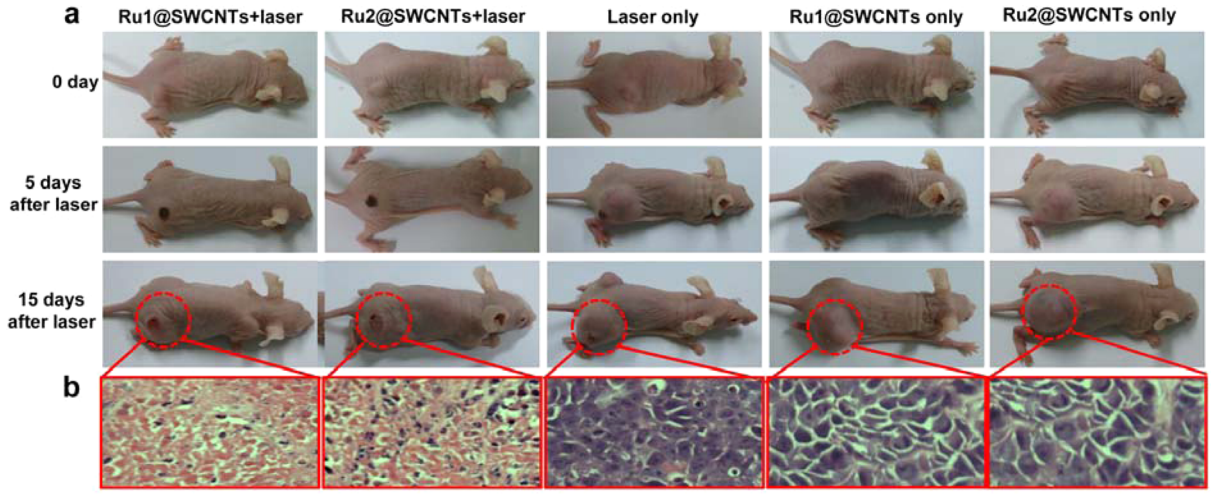

Figure 10. (a) Representative photographs of HeLa tumors in mice with five different treatments (Ru1@SWCNTs + laser; Ru2@SWCNTs + laser; laser only; Ru1@SWCNTs only; Ru1@SWCNTs only). (b) Histological examination of tumors with five treatments on day 15. The power of 808 nm laser was 0.25 W/cm^2.

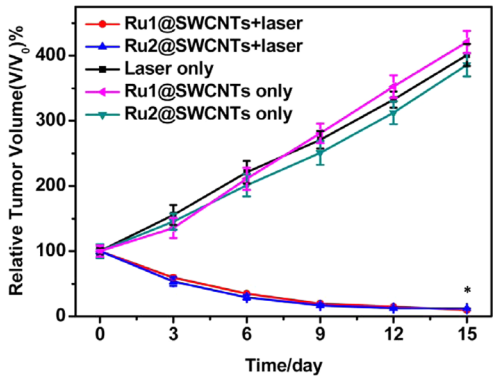

Figure 11. Tumor growth curves for different mice groups after treatment (Irradiation at 808 nm, 0.25 W/cm^2). Tumor volumes were normalized to their initial sizes. Error bars represented the standard deviation of 8 mice per group. Asterisk (*) denotes $p < 0.01$, compared with the physiological saline group on day 0.

CONCLUSION

A bimodal therapy system (Ru@SWCNTs) for PTT and two-photon PDT was successfully fabricated using a facile one-step method by coating Ru(II) complex on the surface of SWCNTs via noncovalent $\pi-\pi$ interaction. In this bimodal PTT–TPPDT system, the photothermal effect of Ru@SWCNTs triggered the release of Ru(II) complexes, the released Ru(II) complexes could produce $^1O_2$ upon 808 nm laser irradiation. The results of *in vitro* cell viability assays showed that the phototherapy effects of Ru@SWCNTs was observably higher than those of free Ru(II) complex and SWCNTs, which indicated that the combined bimodal PTT and TPPDT exhibited better anticancer efficacy. Moreover, *in vivo* tumor ablation was achieved with excellent treatment efficacy under a diode laser (808 nm) irradiation at the power density of 0.25 W/cm^2 for 5 min. These results highlighted that the combined PTT and TPPDT endowed Ru@SWCNTs with high potential for cancer therapy.

EXPERIMENTAL SECTION

Materials. The *cis*-$[Ru(bpy)_2Cl_2]\cdot 2H_2O$ complex[63] was synthesized according to published methods. Ruthenium chloride hydrate (Alfa Aesar, USA), 2,2′-bipyridine (bpy, Sigma–Aldrich, USA), 3-(4,5-dimethylthiazol-2-yl)-2,5-diphenyltetrazolium bromide (MTT, Sigma–Aldrich, USA), Rhodamine B (Sigma–Aldrich, USA), 2′,7′-dichlorofluorescin diacetate (H_2DCF-DA, Sigma–Aldrich), 1,3-diphenyliso-benzofuran (DPBF, Sigma–Aldrich, USA) and SWCNTs (≥90%, 0.7–1.3 nm diameter, Sigma–Aldrich, USA) were used as received. Lyso-Tracker Green was purchased from Invitrogen. Water with a resistivity of 18.2 MΩ cm was used in all experiments and was purified with a Milli-Q system from Millipore Company (Boston, MA, USA). The complex $[\mathbf{Ru(bpy)_2(taptp)}]\mathbf{Cl_2}$ (**Ru1**, **bpy** = 2,2′-bipyridine, **taptp** = 4,5,9,18-tetraazachryseno[9,10-*b*]-triphenylene)[64] and $[\mathbf{Ru(bpy)_2(pdppz)}]\mathbf{Cl_2}$ (**Ru2**, **bpy** = 2,2′-bipyridine, **pdppz** = phenanthro[4,5-abc]dipyrido[3,2-h:2′,3′-j]phenazine)[65] were synthesized as previously described.

General Instruments. Microanalyses (C, H, and N) were carried out on a Vario EL cube elemental analyzer. ^{1}H NMR spectra were recorded on a Varian INOVA500NB NMR spectrometer with $(CD_3)_2SO$ as a solvent at room temperature. All chemical shifts were measured relative to tetramethylsilane (TMS). Electrospray ionization mass spectra (ESI-MS) were recorded on an LCQ system (Finnigan MAT, USA). The morphology and the microstructure of the Ru@SWCNTs were characterized by transmission electron microscopy (TEM) (JEOL Model JEM2010-HR, 200 kV) and energy-dispersive X-ray spectrometry (EDX) (Model S-520/INCA 300, Japan). X-ray photoelectron spectroscopy (XPS, ESCALab250, Thermo VG) was performed with 200 W Al K_R radiation with twin anodes. All core-level XPS spectra were calibrated using a C_{1s} photoelectron peak at 284.6 eV as a reference. The Raman spectra were measured on a Renishawin via Raman microscope and were taken 20 times with exposure times of 10 s at 30% power. UV–vis-NIR spectra were recorded on a spectrophotometer (Shimadzu, Model UV-3150). Emission spectra were recorded on a Perkin–Elmer Model LS55 spectrofluorophotometer at room temperature. Luminescent quantum yields at room temperature (25 °C) were calculated according to published procedures by using an aerated aqueous solution of $[Ru(bpy)_3]^{2+}$ ($\Phi_{em} = 0.028$[47]) as the reference emitter. All data were processed using Origin Pro 7.5 software. A diode laser

DOI: 10.1021/acsami.5b07510
ACS Appl. Mater. Interfaces 2015, 7, 23278–23290

(808 nm) from Hi-Tech Optoelectronics Co., Ltd. (Beijing, China), was used in this study.

Synthesis. A mixture of SWCNTs (1 mg) and Ru(II) complexes (3 mg) was dispersed in water (10 mL) and sonicated for 4 h. During this process, the temperature was kept constant at 25 °C. The as-prepared suspension was centrifuged at 5000*g* for 30 min to remove the largest insoluble aggregates. The supernatant was transferred into a new tube and centrifuged at 20 000*g* for 30 min. To ensure the complete removal of unlinked Ru complex, the obtained sediment was repeatedly dispersed in water under sonication and centrifuged at 20 000*g* three times. This final sediment, denoted as Ru@SWCNTs composite, was used to prepare the Ru@SWCNTs solution. The characteristics of Ru@SWCNTs were compared with SWCNTs dispersed in an aqueous solution of sodium dodecyl sulfate (SDS) ionic surfactants.

ICP-MS Analyzed the Amount of Ru Complex in Ru@SWCNTs. 50 μg/mL of the constructed Ru@SWCNTs before and after laser were completely digested by 5 mL of aqua regia at mild boiling temperatures. The solution was evaporated to 1/3 mL and cooled to room temperature. Subsequently, the sample was diluted to 3% HNO_3 by Milli Q H_2O, and then the amount of Ru was analyzed by inductively coupled plasma mass spectrometry (ICP-MS) (Thermo Elemental Co., Ltd.). Quantification was carried out by external five-point calibration.

Photothermal Measurements. For photothermal measurements, 100 μL of the Ru@SWCNTs solutions at the same concentrations (50 μg/mL) were placed in a series of specimen cuvettes, and each cuvette was irradiated by an 808 nm laser (0.25 W/cm^2, 5 min). Light-induced temperature changes in the solutions were collected using a thermal camera (MAG32, Magnity Electronics, Thermal Imaging Expert). Pure SWCNTs were used as control groups, and three replicates were conducted for each sample.

Photothermal-Triggered Release of Ru(II) Complexes. The release studies were performed at room temperature. Ru@SWCNT solutions were irradiated with an 808 nm laser at an output power of 0.25 W/cm^2 for 5 min. The nanocomposite solutions were pelleted (20 000 rpm, 30 min), and the supernatants were analyzed for the Ru(II) complexes before and after NIR laser irradiation. The concentrations of Ru(II) complexes were determined via spectrophotometry.

Determination of Two-Photon Absorption Cross Sections. The two-photon absorption spectra of probes were determined over a broad spectral range by a typical two-photon induced luminescence (TPL) method, using Rhodamine B in methanol as a standard. The two-photon luminescence data were acquired using an Opolette 355II (pulse width ≤100 fs, 80 MHz repetition rate, tuning range 750−1050 nm, Spectra Physics, Inc., USA). Two-photon luminescence measurements were performed in fluorometric quartz cuvettes. The experimental luminescence excitation and detection conditions were conducted with negligible reabsorption processes, which can affect the TPA measurements. The quadratic dependence of two-photon-induced luminescence intensity on the excitation power was verified at an excitation wavelength of 808 nm. The two-photon absorption cross section of the probes was calculated at each wavelength, according to eq 1:[66]

$$\delta_2 = \delta_1\left(\frac{\phi_1 C_1 I_2 n_2}{\phi_2 C_2 I_1 n_1}\right) \quad (1)$$

where I is the integrated luminescence intensity, C the concentration, n the refractive index, and Φ the quantum yield. Subscript "1" indicates reference samples, and subscript "2" indicates experimental samples.

Reactive Oxygen Species (ROS) Detection. To detect the generation of ROS by Ru(II) complexes under irradiation, 2,2,6,6-tetramethylpiperidine (TEMP) and 5,5-dimethyl-1-pyrroline-*N*-oxide (DMPO) were used as spin trap reagents. Experimental solutions were prepared by mixing 10 μL of Ru(II) complex (50 μg/mL) with 10 μL of DMPO (0.8 M) and 100 μL of PBS (pH 7.0). The solutions were irradiated with an 808 nm laser (0.25 W/cm^2, 80 MHz, 100 fs) for 5 min. Afterward, the solutions were inserted into capillary tubes and placed in the EPR cavity, and the spectra were recorded on a Bruker A300 Spectrometer at 298 K. The measurement conditions were as follows: frequency, 9.8 GHz; microwave power, 19.87 mW; sweep time, 27.65 s; sweep width, 200 G; and modulation frequency, 100 kHz.

Singlet Oxygen Quantum Yields. Indirect Method. A singlet oxygen sensor (DPBF) highly selective for singlet oxygen was used to evaluate the singlet oxygen generation (SOG) of the Ru(II) complex. The Ru(II) complex was irradiated with a 450 nm xenon lamp for different irradiation times. DPBF was dissolved in water containing 2% methanol to a final concentration of 10 μM. DPBF fluorescence emission was produced using an excitation wavelength of 479 nm. The sample SOG was evaluated by comparing the DPBF fluorescence enhancement with those of the background or control samples. DPBF fluorescence emission was produced using an excitation wavelength of 405 nm.

The $^1O_2$ generation quantum yield (Φ_Δ) was calculated according to eqs 2 and 3,[49]

$$\frac{-\Delta[\mathrm{DPBF}]}{t} = \frac{I_0 - I_t}{t} = I_{in}\Phi_{ab}\Phi_\Delta\Phi_r \quad (2)$$

$$\frac{k}{k^s} = \frac{\Phi_{ab}}{\Phi^s_{ab}} = \frac{\Phi_\Delta}{\Phi^s_\Delta} \quad (3)$$

where I_{in} is the incident monochromatic light intensity, Φ_{ab} the light-absorbing efficiency, Φ_r the reaction quantum yield of $^1O_2$ with DPBF (1,3-diphenyl-isobenzofuran), and t the reaction time. I_0 and I_t are the fluorescence intensities of DPBF by the addition of the Ru(II) complex before and after irradiation, respectively; k is the slope, and the superscript "s" refers to the standard. The standard is $[Ru(bpy)_3]^{2+}$ (Φ^s_Δ = 0.22 in D_2O).[48]

Direct Method (Near-Infrared Luminescence). The Ru(II) complex was diluted in D_2O to decrease the absorbance to ~0.2. This solution was then irradiated in fluorescence quartz cuvettes (1 cm width) using a 450 nm xenon lamp. The singlet oxygen near-IR luminescence at 1270 nm was measured by recording spectra from 1050 nm to 1500 nm. The intensity of the irradiation was varied via neutral density filters. Singlet oxygen luminescence peaks at different irradiation intensities were integrated, and the resulting areas were plotted against irradiation intensities. The quantum yields were then calculated by applying the same formulas as those used for the indirect method.

2D Cancer Cell Culture and Cytotoxicity Test. HeLa cancer cell lines and LO2 normal cells were obtained from the Cell Bank (Cell Institute, Sinica Academia Shanghai, Shanghai, China). Cells were routinely maintained in DMEM or RoswellPark Memorial Institute medium (RPMI 1640, Gibco) supplemented with 10% (v/v) fetal bovine serum

DOI: 10.1021/acsami.5b07510
ACS Appl. Mater. Interfaces 2015, 7, 23278−23290

(FBS, Gibco), 50 U/mL streptomycin and 50 ng/mL penicillin. The cancer cells were cultured at 37 °C in an incubator.

To a flat-bottomed 96-well plate, 1×10^4 cells/well were seeded, supplemented with culture medium (100 μL/well), and incubated at 37 °C for 24 h in 5% CO_2/95% air. After adding the serially diluted solutions of Ru@SWCNTs, the cells were incubated for an additional 12 h. The cells were then exposed to an 808 nm laser (0.25 W/cm^2, 80 MHz, 100 fs) for 5 min. The irradiated plates were returned to the incubator for another 12 h. Cell viability was measured with the MTT assay. The optical density of each well was then measured using a spectrophotometer at a wavelength of 590 nm. All cytotoxicity tests were performed in parallel with negative controls, which consisted of cells in the presence of the drugs without irradiation.

Two-Photon-Induced $^1O_2$ Generation in 2D Cancer Cells. The production of intracellular $^1O_2$ was detected by 2′,7′-dichlorofluorescein diacetate (DCFH-DA, Sigma−Aldrich), a cell-permeable nonfluorescent probe that is de-esterified in cells and upon oxidation, changes to highly fluorescent 2′,7′-dichlorofluorescein. HeLa cells were seeded in white 96-well plates at a density of 1×10^4 cells/mL 1 day before treatment. The medium was removed and DCFH-DA (10 μM) was added to cells for 30 min at 37 °C in darkness. The cells were subsequently washed in serum-free medium, treated with Ru(II) complex (50 μg/mL), and then irradiated for 2 min by an 808 nm laser (0.25 W/cm^2, 80 MHz, 100 fs) in the absence or the presence of 10 mM *N*-acetylcysteine (NAC, an antioxidant, Alfa Aesar). The resultant fluorescence was quantified at 530 nm emission with a 488 nm excitation wavelength using a microplate reader (Infinite M200 Pro, Tecan, Männedorf, Switzerland). Fluorescent images were captured using a laser scanning confocal microscope (Carl Zeiss, Model LSM 710). The 510−550 nm emission intensities were recorded at an excitation of 488 nm.

Cellular Uptake. HeLa cell lines were incubated with the Ru@SWCNTs (50 μg/mL) for 1 h at 37 °C and then were costained with Lyso-Tracker Green (2 μM) for 30 min. After being washed with fresh PBS (pH 7.0) three times, the cells were or were not irradiated at 808 nm (0.25 W/cm^2, 80 MHz, 100 fs) for 2 min (the time was decreased because cell death occurs with excessive irradiation exposure, i.e., 5 min). The samples were imaged on a Carl Zeiss LSM 710 NLO confocal microscope (63× oil immersion objective). The excitation wavelength of the Ru(II) complex was 808 nm, and the two-photon images were integrated over the 580−650 nm range.

HeLa cells were treated with the Ru@SWCNTs (50 μg/mL) at 37 °C for 1 h. The cells were washed twice and fixed with 2% glutaraldehyde at 4 °C for 1 h. The cells were then dehydrated with sequential washes in ethanol and embedded in Spurr's resin. The obtained ultrathin sections were mounted in copper grids, counterstained with uranyl acetate and lead citrate, and visualized on an electron microscope (JWOL, Model TEM 100 CX, Tokyo, Japan).

Generation of 3D Multicellular Tumor Spheroids. HeLa multicellular spheroids (MCTSs) were generated using the liquid overlay method.[67] Briefly, the cells were incubated at 37 °C in a 5% CO_2 humidified atmosphere. When the cells reached ∼80% confluence, they were harvested by trypsinization and resuspended in DMEM supplemented with 10% (v/v) FBS. Single cell suspensions were seeded into flat-bottom standard 96-well plates. The wells were previously coated with 50 μL of a sterile 1.0% (w/v) solution of agarose in DMEM to generate a nonadherent surface. To produce multicellular spheroids, 6000 cells suspended in 150 μL of culture media were added into each agarose-coated well, and the plates were incubated for 72 h at 37 °C and 5% humidified CO_2 until spheroids formed. For subsequent drug treatments and imaging procedures, the spheroids were carefully transferred from 96-well plates to fluorodish cell culture dishes. Spheroids with an average diameter of ∼400 μm after 3 days growth were used for the experiments.

The cytotoxicity of Ru(II) complexes toward MCTSs was measured based on the solution ATP concentration with CellTiterGlo kits (Promega).[67] MCTSs of ∼400 μm diameters were treated by carefully replacing 50% of the medium with drug-supplemented standard medium using an 8-channel pipet. In parallel, for the untreated reference MCTSs, we replaced 50% of the medium of the solvent-containing or solvent-free medium. MCTSs were treated with nanoparticles and allowed to incubate for 24 h. Then, the MCTSs were irradiated using a 0.25 W/cm^2 808 nm laser for 5 min. The cytotoxicity of Ru@SWCNTs with laser irradiation toward MCTSs was measured based on the solution ATP concentration with CellTiterGlo kits (Promega). The tests were also performed in parallel with controls, which consisted of cells in the presence of the nanocomposites without irradiation.

Live/Dead Viability Assay. The live/dead assay of MCTSs was performed using the LIVE/DEAD viability/cytotoxicity kit for mammalian cells (Life Technologies). Live cells were distinguished by the presence of ubiquitous intracellular esterase activity, as determined by the enzymatic conversion of the virtually nonfluorescent cell-permeant calcein AM to the intensely fluorescent calcein (λ_{ex} = 488 nm, λ_{em} = 520 ± 20 nm). The determination of cell viability is dependent on these physical and biochemical cell properties. After 2D HeLa cancer cells/MCTS were treated with Ru@SWCNTs and an 808 nm laser irradiation (0.25 W/cm^2, 5 min), the cells (and their respective controls) were incubated with calcein AM (2 μM) solutions for 30 min (2D HeLa cells) or 60 min (MCTS) and imaged directly using an inverted fluorescence microscope (Zeiss, Model Axio Observer D1, Germany).

Photothermal Therapy *In Vivo*. BALB/c-(nu/nu) female nude mice aged 4−5 weeks were purchased and bred in the Center of Experiment Animals at Sun Yat-Sen University. All experimental protocols were approved by the Sun Yat-Sen University Animal Care and Use Committee. HeLa xenografts were established by inoculating 2×10^6 cells via subcutaneous injection (s.c.) into BALB/c-(nu/nu) female nude mice. When the tumor volume reached ∼120 mm^3, the nude mice were randomly allocated into three groups (8 mice per group) before the experiments.

The photothermal therapy process was as follows:

Group 1 (Ru1@SWCNTs + laser): mice were intratumorally injected with the Ru1@SWCNTs (100 μL/20 g body weight of 1 mg/mL solution, a dose of 100 μg Ru1@SWCNTs/20 g body weight), and then irradiated for 5 min;

Group 2 (Ru2@SWCNTs + laser): mice were intratumorally injected with the Ru2@SWCNTs (100 μL/20 g body weight of 1 mg/mL solution, 100 μg Ru2@SWCNTs/20 g body weight), and then irradiated for 5 min;

Group 3 (laser only): mice were only irradiated by laser as a control;

DOI: 10.1021/acsami.5b07510
ACS Appl. Mater. Interfaces 2015, 7, 23278−23290

Group 4 (Ru1@SWCNTs only): mice were intratumorally injected with the Ru1@SWCNTs (100 μL/20 g body weight of 1 mg/mL solution, a dose of 100 μg Ru1@SWCNTs/20 g body weight);
Group 5 (Ru2@SWCNTs only): mice were intratumorally injected with the Ru2@SWCNTs (100 μL/20 g body weight of 1 mg/mL solution, a dose of 100 μg Ru2@SWCNTs/20 g body weight).

Groups 1−3 were irradiated with a diode laser (808 nm, Hi-Tech Optoelectronics Co., Ltd. Beijing, China). Thermal imaging was recorded by a thermal camera (MAG30, Magnity Electronics, Thermal Imaging Expert) when the tumors were exposed to a 808 nm laser with a power density at 0.25 W/cm^2 for 5 min.

After the irradiation (day 0), the tumor sizes were measured using a caliper every 3 days. The mice with tumors were photographed with a digital color camera at day 0, day 5, and day 15. The tumor volumes were calculated based on the following formula:

$$\text{tumor volume (V)} = \frac{(\text{tumor length}) \times (\text{tumor width})^2}{2}$$

The relative tumor volumes were calculated as V/V_0, where V_0 was the initial tumor volume at day 0.

Histological Examination. At the end of the photothermal therapy *in vivo*, all the mice of the three groups were sacrificed and the organs (including liver, kidney, spleen, heart, lung, brain, intestine, and ovaries) and tumor tissue were resected. A portion of these fresh tissues were immersed in 4% paraformaldehyde at 4 °C. For morphological studies, 6 μm sections were obtained from paraffin-embedded samples, processed according to the standard procedures for inclusion, and rehydrated (xylene, alcohol, water). Sections were stained with hematoxylin-eosin (H&E). (Hematoxylin has a deep blue-purple color and stains nucleic acids; eosin is pink and stains proteins nonspecifically.) In a typical tissue, nuclei are stained blue, whereas the cytoplasm and extracellular matrix have varying degrees of pink staining. The sections were observed with an Olympus microscope to analyze the tissue structure and cell state.

Statistical Analysis. Data were presented in the form of mean ± standard deviation, and significance was assessed uaing a Student's *t*-test. Differences were considered to be significant at $P < 0.05$.

■ ASSOCIATED CONTENT

Supporting Information

The Supporting Information is available free of charge on the ACS Publications website at DOI: 10.1021/acsami.5b07510.

ICP-MS measurement of Ru@SWCNTs; schematic presentations of Ru@SWCNTs; characterization of Ru@SWCNTs; stability of Ru@SWCNTs; XPS spectra of the Ru@SWCNTs; photothermal images of Ru@SWCNTs, as a function of laser power; the absorption spectra of Ru@SWCNTs before and after irradiation; the luminescence spectra of the Ru@SWNTs; two-photon properties of Ru(II) complexes; EPR signals of ROS of Ru2 complex; the emission spectra changes of DPBF−Ru system; measurement of intracellular $^1O_2$; cellular uptaken analysis; viability of LO2 normal cells; viability of HeLa cancer cells; live/dead viability assay; tumor growth curves *in vivo* of the body weights of mice after various treatments; histological examination of primary organs (PDF)

■ AUTHOR INFORMATION

Corresponding Author

*Tel: +86-20-86110613. Fax: +86-20-84112245. E-mail: ceschh@mail.sysu.edu.cn.

Notes

The authors declare no competing financial interest.

■ ACKNOWLEDGMENTS

This work was supported by the 973 Program (Nos. 2014CB845604 and 2015CB856301), the National Science Foundation of China (Nos. 21172273, 21171177, 21471164, and J1103305), and Program for Changjiang Scholars and Innovative Research Team in University of China (No. IRT1298).

■ REFERENCES

(1) Greco, F.; Vicent, M. J. Combination Therapy: Opportunities and Challenges for Polymer−Drug Conjugates as Anticancer Nanomedicines. *Adv. Drug Delivery Rev.* **2009**, *61*, 1203−1213.
(2) Lane, D. Designer Combination Therapy for Cancer. *Nat. Biotechnol.* **2006**, *24*, 163−164.
(3) Sengupta, S.; Eavarone, D.; Capila, I.; Zhao, G.; Watson, N.; Kiziltepe, T.; Sasisekharan, R. Temporal Targeting of Tumour Cells and Neovasculature with a Nanoscale Delivery System. *Nature* **2005**, *436*, 568−572.
(4) Sun, T. M.; Du, J. Z.; Yao, Y. D.; Mao, C. Q.; Dou, S.; Huang, S. Y.; Zhang, P.-Z.; Leong, K. W.; Song, E.-W.; Wang, J. Simultaneous Delivery of siRNA and Paclitaxel via a "two-in-one" Micelleplex Promotes Synergistic Tumor Suppression. *ACS Nano* **2011**, *5*, 1483−1494.
(5) Liu, H. Y.; Chen, D.; Li, L. L.; Liu, T. L.; Tan, L. F.; Wu, X.; Tang, F. Multifunctional Gold Nanoshells on Silica Nanorattles: A Platform for the Combination of Photothermal Therapy and Chemotherapy with Low Systemic Toxicity. *Angew. Chem., Int. Ed.* **2011**, *50*, 891−895.
(6) Phillips, D. Light Relief: Photochemistry and Medicine. *Photochem. Photobiol. Sci.* **2010**, *9*, 1589−1596.
(7) Velusamy, M.; Shen, J. Y.; Lin, J. T.; Lin, Y. C.; Hsieh, C. C.; Lai, C. H.; Lai, C.-W.; Ho, M.-L.; Chen, Y.-C.; Chou, P.-T.; Hsiao, J.-K. A New Series of Quadrupolar Type Two-photon Absorption Chromophores Bearing 11, 12-dibutoxydibenzo[a,c]-phenazine bridged amines; Their Applications in Two-photon Fluorescence Imaging and Two-photon Photodynamic Therapy. *Adv. Funct. Mater.* **2009**, *19*, 2388−2397.
(8) Mari, C.; Pierroz, V.; Ferrari, S.; Gasser, G. Combination of Ru(II) Complexes and Light: New Frontiers in Cancer Therapy. *Chem. Sci.* **2015**, *6*, 2660−2686.
(9) Gary-Bobo, M.; Mir, Y.; Rouxel, C.; Brevet, D.; Basile, I.; Maynadier, M.; Vaillant, O.; Mongin, O.; Blanchard-Desce, M.; Morère, A.; Garcia, M.; Durand, J. O.; Raehm, L. Mannose-functionalized Mesoporous Silica Nanoparticles for Efficient Two-photon Photodynamic Therapy of Solid Tumors. *Angew. Chem., Int. Ed.* **2011**, *50*, 11425−11429.
(10) Choi, K. Y.; Liu, G.; Lee, S.; Chen, X. Theranostic Nanoplatforms for Simultaneous Cancer Imaging and Therapy: Current Approaches and Future Perspectives. *Nanoscale* **2012**, *4*, 330−342.
(11) Jaque, D.; Martinez Maestro, L.; del Rosal, B.; Haro-Gonzalez, P.; Benayas, A.; Plaza, J. L.; Martin Rodríguez, E.; Garcia Solé, J. Nanoparticles for Photothermal Therapies. *Nanoscale* **2014**, *6*, 9494−9530.
(12) Muzi, L.; Menard-Moyon, C.; Russier, J.; Li, J.; Chin, C. F.; Ang, W. H.; Pastorin, G.; Risuleo, G.; Bianco, A. Diameter-dependent

Release of a Cisplatinpro-drug from Small and Large Functionalized Carbon Nanotubes. *Nanoscale* **2015**, *7*, 5383−5394.
(13) Battigelli, A.; Russier, J.; Venturelli, E.; Fabbro, C.; Petronilli, V.; Bernardi, P.; Da Ros, T.; Prato, M.; Bianco, A. Peptide-based Carbon Nanotubes for Mitochondrial Targeting. *Nanoscale* **2013**, *5*, 9110−9117.
(14) Wang, N.; Feng, Y. X.; Zeng, L. L.; Zhao, Z. N.; Chen, T. F. Functionalized Multiwalled Carbon Nanotubes as Carriers of Ruthenium Complexes to Antagonize Cancer Multidrug Resistance and Radioresistance. *ACS Appl. Mater. Interfaces* **2015**, *7*, 14933−14945.
(15) Heister, E.; Brunner, E. W.; Dieckmann, G. R.; Jurewicz, I.; Dalton, A. B. Are Carbon Nanotubes a Natural Solution? Applications in Biology and Medicine. *ACS Appl. Mater. Interfaces* **2013**, *5*, 1870−1891.
(16) Kam, N. W. S.; Dai, H. Carbon Nanotubes as Intracellular Protein Transporters: Generality and Biological Functionality. *J. Am. Chem. Soc.* **2005**, *127*, 6021−6026.
(17) Singh, R.; Pantarotto, D.; McCarthy, D.; Chaloin, O.; Hoebeke, J.; Partidos, C. D.; Briand, J.-P.; Prato, M.; Bianco, A.; Kostarelos, K. Binding and Condensation of Plasmid DNA onto Functionalized Carbon Nanotubes: Toward the Construction of Nanotube-based Gene Delivery Vectors. *J. Am. Chem. Soc.* **2005**, *127*, 4388−4396.
(18) Bianco, A.; Kostarelos, K.; Prato, M. Application of Carbon Nanotubes in Drug Delivery. *Curr. Opin. Chem. Biol.* **2005**, *9*, 674−679.
(19) Bianco, A.; Kostarelos, K.; Partidos, C. D.; Prato, M. Biomedical Application of Functionalised Carbon Nanotubes. *Chem. Commun.* **2005**, *5*, 571−577.
(20) Wu, W.; Wieckowski, S.; Pastorin, G.; Benincasa, M.; Klumpp, C.; Briand, J.-P.; Gennaro, R.; Prato, M.; Bianco, A. Targeted Delivery of Amphotericin B to Cells by Using Functionalized Carbon Nanotubes. *Angew. Chem., Int. Ed.* **2005**, *44*, 6358−6362.
(21) Shi Kam, N. W.; O'Connell, M.; Wisdom, J. A.; Dai, H. Carbon Nanotubes as Multifunctional Biological Transporters and Near-infrared Agents for Selective Cancer Cell Destruction. *Proc. Natl. Acad. Sci. U. S. A.* **2005**, *102*, 11600−11605.
(22) Dougherty, T. J.; Kaufman, J. E.; Goldfarb, A.; Weishaupt, K. R.; Boyle, D.; Mittleman, A. Photoradiation Therapy for the Treatment of Malignant Tumors. *Cancer Res.* **1978**, *3*, 2628−2635.
(23) Dougherty, T. J.; Gomer, C. J.; Henderson, B. W.; Jori, G.; Kessel, D.; Korbelik, M.; Moan, J.; Peng, Q. Photodynamic Therapy. *J. Natl. Cancer Inst.* **1998**, *90*, 889−905.
(24) Moan, J. Porphyrin Photosensitization and Phototherapy. *Photochem. Photobiol.* **1986**, *43*, 681−690.
(25) Man, B. Y. W.; Chan, H. M.; Leung, C. H.; Chan, D. S. H.; Bai, L. P.; Jiang, Z. H.; Li, H. W.; Ma, D. L. Group 9 Metal-based Inhibitors of β-amyloid (1−40) Fibrillation as Potential Therapeutic Agents for Alzheimer's Disease. *Chem. Sci.* **2011**, *2*, 917−921.
(26) Leung, C. H.; Zhong, H. J.; Yang, H.; Cheng, Z.; Chan, D. S. H.; Ma, V. P. Y.; Abagyan, R.; Wong, C. Y.; Ma, D. L. A Metal-Based Inhibitor of Tumor Necrosis Factor-α. *Angew. Chem., Int. Ed.* **2012**, *51*, 9010−9014.
(27) Ma, D. L.; Liu, L. J.; Leung, K. H.; Chen, Y. T.; Zhong, H. J.; Chan, D. S.; Wang, H. M.; Leung, C. H. Antagonizing STAT3 Dimerization with a Rhodium(III) Complex. *Angew. Chem., Int. Ed.* **2014**, *53*, 9178−9182.
(28) Frei, A.; Rubbiani, R.; Tubafard, S.; Blacque, O.; Anstaett, P.; Felgenträger, A.; Maisch, T.; Spiccia, L.; Gasser, G. Synthesis, Characterization, and Biological Evaluation of New Ru(II) Polypyridyl Photosensitizers for Photodynamic Therapy. *J. Med. Chem.* **2014**, *57*, 7280−7292.
(29) Mari, C.; Pierroz, V.; Rubbiani, R.; Patra, M.; Hess, J.; Spingler, B.; Oehninger, L.; Schur, J.; Ott, I.; Salassa, L.; Ferrari, S.; Gasser, G. DNA Intercalating Ru(II) Polypyridyl Complexes as Effective Photosensitizers in Photodynamic Therapy. *Chem. - Eur. J.* **2014**, *20*, 14421−14436.
(30) Pierroz, V.; Joshi, T.; Leonidova, A.; Mari, C.; Schur, J.; Ott, I.; Spiccia, L.; Ferrari, S.; Gasser, G. Molecular and Cellular Characterization of the Biological Effects of Ruthenium(II) Complexes Incorporating 2-pyridyl-2-pyrimidine-4-carboxylic Acid. *J. Am. Chem. Soc.* **2012**, *134*, 20376−20387.
(31) Lincoln, R.; Kohler, L.; Monro, S.; Yin, H.; Stephenson, M.; Zong, R.; Chouai, A.; Dorsey, C.; Hennigar, R.; Thummel, R. P.; McFarland, S. A. Exploitation of Long-lived 3IL Excited States for Metal−organic Photodynamic Therapy: Verification in a Metastatic Melanoma Model. *J. Am. Chem. Soc.* **2013**, *135*, 17161−17175.
(32) Zhang, P.; Pei, L.; Chen, Y.; Xu, W.; Lin, Q.; Wang, J.; Wu, J.; Shen, Y.; Ji, L.; Chao, H. A Dinuclear Ruthenium(II) Complex as a One- and Two-photon Luminescent Probe for Biological Cu^{2+} Detection. *Chem. - Eur. J.* **2013**, *19*, 15494−15503.
(33) Zhang, P.; Wang, J.; Huang, H.; Chen, H.; Guan, R.; Chen, Y.; Ji, L. N.; Chao, H. RuNH2@AuNPs as Two-photon Luminescent Probes for Thiols in Living Cells and Tissues. *Biomaterials* **2014**, *35*, 9003−9011.
(34) Xu, W.; Zuo, J.; Wang, L.; Ji, L.; Chao, H. Dinuclear Ruthenium(II) Polypyridyl Complexes as Single and Two-photon Luminescence Cellular Imaging Probes. *Chem. Commun.* **2014**, *50*, 2123−2125.
(35) Jiang, B. P.; Hu, L. F.; Wang, D. J.; Ji, S. C.; Shen, X. C.; Liang, H. Graphene Loading Water-soluble Phthalocyanine for Dual-modality Photothermal/Photodynamic Therapy via a One-step Method. *J. Mater. Chem. B* **2014**, *2*, 7141−7148.
(36) Jiang, B. P.; Hu, L. F.; Shen, X. C.; Ji, S. C.; Shi, Z. J.; Liu, C. J.; Zhang, L.; Liang, H. One-step Preparation of a Water-soluble Carbon Nanohorn/Phthalocyanine Hybrid for Dual-Modality Photothermal and Photodynamic Therapy. *ACS Appl. Mater. Interfaces* **2014**, *6*, 18008−18017.
(37) Hessel, C. M.; Pattani, V. P.; Rasch, M.; Panthani, M. G.; Koo, B.; Tunnell, J. W.; Korgel, B. A. Copper Selenide Nanocrystals for Photothermal Therapy. *Nano Lett.* **2011**, *11*, 2560−2566.
(38) Huang, P.; Lin, J.; Li, W. W.; Rong, P. F.; Wang, Z.; Wang, S. J.; Wang, X. P.; Sun, X. L.; Aronova, M.; Niu, G.; Leapman, R. D.; Nie, Z. H.; Chen, X. Y. Biodegradable Gold Nanovesicles with an Ultrastrong Plasmonic Coupling Effect for Photoacoustic Imaging and Photothermal Therapy. *Angew. Chem., Int. Ed.* **2013**, *52*, 13958−13964.
(39) Tian, Q. W.; Jiang, F. R.; Zou, R. J.; Liu, Q.; Chen, Z. G.; Zhu, M. F.; Yang, S. P.; Wang, J. L.; Wang, J. H.; Hu, J. Q. Hydrophilic Cu_9S_5 Nanocrystals: A Photothermal Agent with a 25.7% Heat Conversion Efficiency for Photothermal Ablation of Cancer Cells in Vivo. *ACS Nano* **2011**, *5*, 9761−9771.
(40) Lin, J.; Wang, S.; Huang, P.; Wang, Z.; Chen, S.; Niu, G.; Li, W.; He, J.; Cui, D.; Lu, G.; Chen, X.; Nie, Z. Photosensitizer-loaded Gold Vesicles with Strong Plasmonic Coupling Effect for Imaging-Guided Photothermal/Photodynamic Therapy. *ACS Nano* **2013**, *7*, 5320−5329.
(41) Huang, X. H.; El-Sayed, I. H.; Qian, W.; El-Sayed, M. A. Cancer Cell Imaging and Photothermal Therapy in the Near-infrared Region by Using Gold Nanorods. *J. Am. Chem. Soc.* **2006**, *128*, 2115−2120.
(42) Ke, H.; Wang, J.; Dai, Z. F.; Jin, Y.; Qu, E.; Xing, Z.; Guo, C.; Yue, X.; Liu, C. Gold-nanoshelled Microcapsules: a Theranostic Agent for Ultrasound Contrast Imaging and Photothermal Therapy. *Angew. Chem., Int. Ed.* **2011**, *50*, 3017−3021.
(43) Li, W.; Rong, P.; Yang, K.; Huang, P.; Sun, K.; Chen, X. Semimetal Nanomaterials of Antimony as Highly Efficient Agent for Photoacoustic Imaging and Photothermal Therapy. *Biomaterials* **2015**, *45*, 18−26.
(44) Li, B.; Ye, K.; Zhang, Y.; Qin, J.; Zou, R.; Xu, K.; Huang, X.; Xiao, Z.; Zhang, W.; Lu, X.; Hu, J. Photothermal Theragnosis Synergistic Therapy Based on Bimetal Sulphide Nanocrystals Rather Than Nanocomposites. *Adv. Mater.* **2015**, *27*, 1339−1345.
(45) Liu, J.; Zheng, X.; Yan, L.; Zhou, L.; Tian, G.; Yin, W.; Wang, L.; Liu, Y.; Hu, Z.; Gu, Z.; Chen, C.; Zhao, Y. Bismuth Sulfide Nanorods as a Precision Nanomedicine for *In Vivo* Multimodal Imaging-guided Photothermal Therapy of Tumor. *ACS Nano* **2015**, *9*, 696−707.
(46) Tian, Q.; Hu, J.; Zhu, Y.; Zou, R.; Chen, Z.; Yang, S.; Li, R.; Su, Q.; Han, Y.; Liu, X. Sub-10 nm Fe_3O_4@$Cu_{(2-x)}S$ Core-shell

DOI: 10.1021/acsami.5b07510
ACS Appl. Mater. Interfaces 2015, 7, 23278−23290

Nanoparticles for Dual-modal Imaging and Photothermal Therapy. *J. Am. Chem. Soc.* **2013**, *135*, 8571−8577.
(47) Juris, A.; Balzani, V.; Barigelletti, F.; Campagna, S.; Belser, P.; Von Zelewsky, A. Ruthenium(II) Polypyridine Complexes: Photophysics, Photochemistry, Electrochemistry, and Chemiluminescence. *Coord. Chem. Rev.* **1988**, *84*, 85−277.
(48) García-Fresnadillo, D.; Georgiadou, Y.; Orellana, G.; Braun, A. M.; Oliveros, E. Singlet-oxygen ($^1\Delta_g$) Production by Rutheniurn(II) Complexes Containing Polyazaheterocyclic Ligands in Methanol and in Water. *Helv. Chim. Acta* **1996**, *79*, 1222−1238.
(49) Yu, H. J.; Huang, S. M.; Li, L. Y.; Jia, H. N.; Chao, H.; Mao, Z. W.; Liu, J. Z.; Ji, L. N. Synthesis, DNA-binding and Photocleavage Studies of Ruthenium Complexes $[Ru(bpy)_2(mitatp)]^{2+}$ and $[Ru(bpy)_2(nitatp)]^{2+}$. *J. Inorg. Biochem.* **2009**, *103*, 881−890.
(50) Drobizhev, M.; Stepanenko, Y.; Dzenis, Y.; Karotki, A.; Rebane, A.; Taylor, P. N.; Anderson, H. L. Extremely Strong Near-IR Two-photon Absorption in Conjugated Porphyrin Dimers: Quantitative Description with Three-essential-states Model. *J. Phys. Chem. B* **2005**, *109*, 7223−7236.
(51) Ishi-i, T.; Taguri, Y.; Kato, S.; Shigeiwa, M.; Gorohmaru, H.; Maeda, S.; Mataka, S. Singlet Oxygen Generation by Two-photon Excitation of Porphyrin Derivatives Having Two-photon-Absorbing Benzothiadiazole Chromophores. *J. Mater. Chem.* **2007**, *17*, 3341−3346.
(52) Hamilton, G. Multicellular Spheroids as an in Vitro Tumor Model. *Cancer Lett.* **1998**, *131*, 29−34.
(53) Pampaloni, F.; Reynaud, E. G.; Stelzer, E. H. K. The Third Dimension Bridges the Gap Between Cell Culture and Live Tissue. *Nat. Rev. Mol. Cell Biol.* **2007**, *8*, 839−845.
(54) Dmitriev, R. I.; Zhdanov, A. V.; Nolan, Y. M.; Papkovsky, D. B. Imaging of Neurosphere Oxygenation with Phosphorescent Probes. *Biomaterials* **2013**, *34*, 9307−9317.
(55) Ho, V. H. B.; Slater, N. K. H.; Chen, R. J. PH-responsive Endosomolytic Pseudo-peptides for Drug Delivery to Multicellular Spheroids Tumour Models. *Biomaterials* **2011**, *32*, 2953−2958.
(56) Wang, X.; Zhen, X.; Wang, J.; Zhang, J. L.; Wu, W.; Jiang, X. Q. Doxorubicin Delivery to 3D Multicellular Spheroids and Tumors Based on Boronic Acid-rich Chitosan Nanoparticles. *Biomaterials* **2013**, *34*, 4667−4679.
(57) Kim, T. H.; Mount, C. W.; Gombotz, W. R.; Pun, S. H. The Delivery of Doxorubicin to 3D Multicellular Spheroids and Tumors in a Murine Xenograft Model Using Tumor-Penetrating Triblock Polymeric Micelles. *Biomaterials* **2010**, *31*, 7386−7397.
(58) Zhou, M.; Zhang, R.; Huang, M.; Lu, W.; Song, S.; Melancon, M. P.; Tian, M.; Liang, D.; Li, C. A Chelator-free Multifunctional [^{64}Cu]CuS Nanoparticle Platform for Simultaneous micro-PET/CT Imaging and Photothermal Ablation Therapy. *J. Am. Chem. Soc.* **2010**, *132*, 15351−15358.
(59) Xie, H.; Goins, B.; Bao, A.; Wang, Z. J.; Phillips, W. T. Effect of Intratumoral Administration on Biodistribution of ^{64}Cu-labeled Nanoshells. *Int. J. Nanomed.* **2012**, *7*, 2227−2238.
(60) Albanese, A.; Tang, P. S.; Chan, W. C. The Effect of Nanoparticle Size, Shape, and Surface Chemistry on Biological Systems. *Annu. Rev. Biomed. Eng.* **2012**, *14*, 1−16.
(61) De Jong, W. H.; Hagens, W. I.; Krystek, P.; Burger, M. C.; Sips, A. J. A. M.; Geertsma, R. E. Particle Size-dependent Organ Distribution of Gold Nanoparticles after Intravenous Administration. *Biomaterials* **2008**, *29*, 1912−1919.
(62) Huang, X. H.; Peng, X. H.; Wang, Y. Q.; Wang, Y. X.; Shin, D. M.; El-Sayed, M. A.; Nie, S. M. A Reexamination of Active and Passive Tumor Targeting by Using Rod-Shaped Gold Nanocrystals and Covalently Conjugated Peptide Ligands. *ACS Nano* **2010**, *4*, 5887−5896.
(63) Sullivan, B. P.; Salmon, D. J.; Meyer, T. J. Mixed Phosphine 2,2′-bipyridine Complexes of Ruthenium. *Inorg. Chem.* **1978**, *17*, 3334−3341.
(64) Liu, Y.; Chouai, A.; Degtyareva, N. N.; Lutterman, D. A.; Dunbar, K. R.; Turro, C. Chemical Control of the DNA Light Switch: Cycling the Switch ON and OFF. *J. Am. Chem. Soc.* **2005**, *127*, 10796−1079.
(65) Gao, F.; Chen, X.; Wang, J.; Chen, Y.; Chao, H.; Ji, L. *In vitro* Transcription Inhibition by Ruthenium(II) Polypyridyl Complexes with Electropositive Ancillary Ligands. *Inorg. Chem.* **2009**, *48*, 5599−5601.
(66) Xu, C.; Webb, W. W. Measurement of Two-photon Excitation Cross Sections of Molecular Fluorophores with Data from 690 to 1050 nm. *J. Opt. Soc. Am. B* **1996**, *13*, 481−491.
(67) Huang, H.; Zhang, P.; Yu, B.; Chen, Y.; Wang, J.; Ji, L.; Chao, H. Targeting Nucleus DNA with a Cyclometalated Dipyridophenazine Ruthenium(II) Complex. *J. Med. Chem.* **2014**, *57*, 8971−8983.

DOI: 10.1021/acsami.5b07510
ACS Appl. Mater. Interfaces 2015, 7, 23278−23290